Laser induced lifetime degradation in p-type crystalline silicon

M. Ametowobla, G. Bilger, J. R. Köhler, and J. H. Werner
Institut für Photovoltaik, Universität Stuttgart, Pfaffenwaldring 47, 70569 Stuttgart, Germany

(Received 2 April 2012; accepted 23 April 2012; published online 13 June 2012)

Pulsed, green laser irradiation of uncoated p-type silicon leads to a significant reduction of the effective minority carrier lifetime. The reason for the lifetime drop lies in the introduction of recombination centres into the laser melted and recrystallized surface layer, leading to a low local minority carrier lifetime $\tau \approx 10$ ns inside this surface layer. The laser treatment introduces the impurities oxygen, carbon and nitrogen into the silicon and further leads to an n-type doping of the surface layer. There are strong indications that these impurities are responsible for the observed n-type doping, as well as the lifetime reduction after irradiation. Both effects are removed by thermal annealing. An estimate shows that the low local lifetime does nevertheless not affect the performance of industrial or contacted selective solar cell emitter structures. © *2012 American Institute of Physics*. [http://dx.doi.org/10.1063/1.4725191]

INTRODUCTION

For more than four decades, the use of lasers for processing semiconductors, particularly laser doping of silicon has been subject of numerous studies. A first peak of attention existed during the early 1980s, when experiments regarding laser doping[1–3] and laser annealing of silicon[4,5] were performed with different laser types and experimental setups by a number of authors. Also, solar cells were fabricated with this technique. However, in spite of the strong initial attention, laser doping did not find its way into industrial production processes, as there was no inherent advantage over the well known furnace diffusion processes. Apart from the characterization of laser doping, there exist studies dealing with the impact of laser irradiation on the lifetime inside irradiated pn-junction diodes and metal oxide semiconductor (MOS) capacitors,[6] as well as the incorporation of impurities into silicon due to laser irradiation.[7,8] However, all of these studies only focus on a narrow section of the whole topic.

Only in recent years, the use of lasers for silicon photovoltaics has regained strong interest. Above all, the necessity to achieve higher efficiencies in order to push down the cost of photovoltaic energy conversion has led to advanced cell concepts like selective emitters[9] or back junction cells,[10] all of which require locally doped areas. Here, the nature of the laser as a local process tool in contrast to the standard diffusion processes gives an inherent advantage, which has enabled the laser doped selective emitter to enter industrial mass production.[11]

For a thorough characterization of the process, our institute has investigated laser doping of complete solar cell emitters, as well as the mere impact of laser irradiation on the material without any additional dopants involved. It was shown by transmission electron microscopy (TEM) that using a specifically tailored focus avoids the formation of crystal defects during the rapid melting and recrystallization process.[12,13] The absence of crystal defects was corroborated by defect etching and x-ray topography (XT).[14] Furthermore, some evidence was given a possible link between impurity incorporation and recombination in the laser treated layers.[15]

This paper extends the existing studies regarding the effects of the laser irradiation and gives new evidence indicating that indeed impurity incorporation and not structural damage to the crystal is correlated to the observed lifetime reduction in the case of the employed laser doping process. It further estimates the local lifetime inside the laser treated surface layers and uses this data to assess the impact of the laser induced defects on the laser treatment of solar cell emitters. For doing so, p-type crystalline silicon samples without any further doping layers are investigated using lifetime measurements, Fourier transformed infrared spectrometry (FTIR), photoluminescense (PL), electrochemical capacitance voltage (ECV) profiling, and secondary ion mass spectrometry (SIMS) characterization.

Lifetime measurements

For the lifetime measurements, four sets (A-D) of high quality float zone (FZ) silicon wafers with base doping concentrations $2.2 \times 10^{15}\ \text{cm}^{-3} < N_A < 1.5 \times 10^{16}\ \text{cm}^{-3}$ are used. A pulsed Nd:YVO_4 laser emitting radiation at a wavelength $\lambda = 532$ nm, with a pulse duration $\tau_p \approx 15$ ns, irradiates the clean sample surfaces. Samples A-C receive irradiation on the front side, whereas samples D are treated on the front and back side. A special optics projects the Gaussian circular laser beam into an elongated cylindrical focus with long axis (semimajor) $l \approx 300\ \mu$m and short axis (semiminor) $w \approx 5\ \mu$m. The samples are supported and moved by an xy-gantry, which enables the processing of larger areas. The translation speed v_y along the semiminor of the focus together with the laser pulse repetition frequency f_p determine the number of melting cycles N_{melt}, every point on the sample surface undergoes as $N_{melt} = w/(v_y/f_p)$, with w given in mm, v_y in mm/s, and f_p in Hz.

The quantity D_p denotes the pulse energy density averaged over the total area of the focus. The experiment varies pulse energy densities D_p as well as melt repetitions N_{melt}. To be able to separate irradiation induced effects from possible experimental problems, three quarters of every wafer are processed with one quarter untreated, serving as a reference.

 © 2012 American Institute of Physics

TABLE I. Experimental parameters for sample sets A-D. Samples A-C are irradiated on one side, whereas samples D are irradiated on both sides.

Series	Doping concentration N_A [cm^{-3}]	Thickness [μm]	Parameter	Process
A	2.2×10^{15}	525	N_{melt}	Single sided
B	5×10^{15}	300	N_{melt}	Single sided
C	1.5×10^{16}	300	N_{melt}	Single sided
D	1.5×10^{16}	300	D_p	Double sided

Table I comprises the experimental conditions for sample sets A-D.

After the irradiation, the samples undergo an RCA (Ref. 16) cleaning step before receiving a high quality silicon nitride (SiN_x) passivation layer with refractive index $n_r \approx 3.0$ consecutively on both sides. Following passivation, the samples are cleaved into quarters and their effective minority carrier lifetime τ_{eff} is determined with a WC-120 Quasi Steady State Photoconductive Decay (QSSPC) measuring setup from Sinton Consulting®.

Figure 1 shows the lifetime τ_{eff} of sample sets A-C versus the number of melting cycles, at one sun illumination. Regardless of the substrate doping density N_A, all three curves show a virtually monotonous decrease of the effective minority carrier lifetime τ_{eff} with a mounting number of melting cycles. The drop ranges from 1848 μs (untreated) to 970 μs ($N_{melt} = 20$) for $N_A = 2.2 \times 10^{15}$ cm^{-3}, from 1310 μs to 439 μs for $N_A = 5 \times 10^{15}$ cm^{-3} (only up to $N_{melt} = 8$), and from 485 μs to 29 μs for $N_A = 1.5 \times 10^{16}$ cm^{-3}. As is seen from the graph, the succession of the three curves reflects the succession of the respective bulk lifetimes, with the highest lifetimes exhibited by the samples with the lowest bulk doping concentration. In addition, also the level of lifetime degradation corresponds to N_A, as the minimum $\tau_{eff} = 970$ μs of series A represents approximately 52% of the reference lifetime, whereas τ_{eff} drops down to only 6% of the reference for series C. While one would expect a low substrate doping

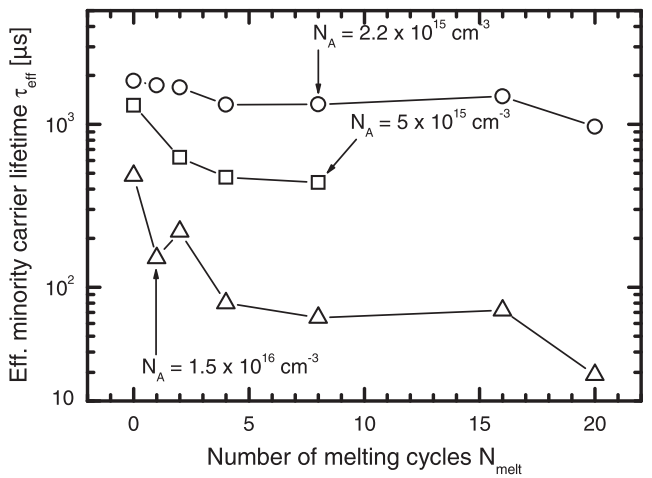

FIG. 1. The carrier lifetimes exhibit a virtually monotonous reduction for all three substrate doping levels. The reduction ranges from 1850 $\mu s > \tau_{eff} > 970 \mu s$ ($N_A = 2.2 \times 10^{15}$ cm^{-3}), 1310 $\mu s > \tau_{eff} > 439$ μs ($N_A = 5 \times 10^{15}$ cm^{-3}), and 485 $\mu s > \tau_{eff} > 29$ μs ($N_A = 1.5 \times 10^{16}$ cm^{-3}).

allowing for higher lifetimes due to lower levels of Auger recombination, the fact that also the sensitivity towards laser treatment seems to be linked to the substrate doping is somehow surprising. A discussion of this effect is given below.

Figure 2 shows the effective minority carrier lifetime τ_{eff} of samples irradiated with $0.3\,J/cm^2 < D_p < 2.8\,J/cm^2$ and 2 or 20 melt repetitions. Likewise, with mounting D_p, the effective carrier lifetime τ_{eff} decreases monotonically. From Ref. 14, we know that the threshold pulse energy density for the melting of silicon $E_{th} \approx 1\,J/cm^2$ with the type of laser used for this study. This threshold is in accordance with the value of $\tau_{eff} = 498$ μs for $N_{melt} = 2$ and $D_p = 0.3\,J/cm^2$ being higher than the reference value, showing that no melting occurred for this low pulse energy density. While the decay is rather linear for the series with two melt repetitions, it is much more pronounced for $N_{melt} = 20$, dropping down to only $\tau_{eff} = 6$ μs for $D_p > 1.9\,J/cm^2$.

Surface layer removal

Apparently, the laser irradiation degrades the minority carrier lifetime inside the samples. In an earlier study,[14] we showed that the laser induced defects are confined to the surface layer, which is melted by the irradiation. In principle, there exist three possibilities for the formation of defects:

- The irradiation probably increases the surface defect state density D_{it}. If the lifetime reduction was solely caused by an increased D_{it}, removing only a few nm from the surface should suffice to remedy the drop in τ_{eff}.
- Possibly a large number of defects is introduced just at the interface between the unaffected bulk and the recrystallized surface layer. As the process involves a phase change from solid to liquid and vice versa, there exists a rather sharp boundary. If this phenomenon was the main reason for the lifetime reduction, a step like increase of the

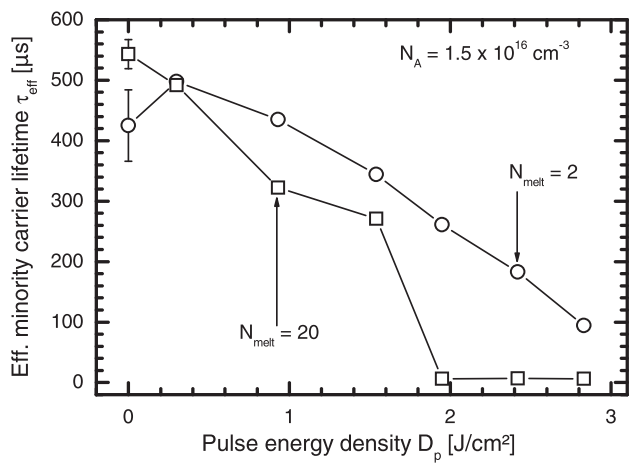

FIG. 2. The carrier lifetime monotonically decreases with increasing laser pulse energy density for both $N_{melt} = 2$ or 20. For two melt repetitions, the lifetime at a low $D_p = 0.3\,J/cm^2$ even exceeds the lifetime of the untreated sample slightly. This low pulse energy density lies below the threshold for laser melting, which ranges at $D_p \approx 1\,J/cm^2$. The lifetime reduction for this parameter set is virtually linear, reaching values as low as $\tau_{eff} \approx 100$ μs for $D_p = 2.8\,J/cm^2$, whereas for $N_{melt} = 20$, a large drop in τ_{eff} can be seen for $D_p > 1.9\,J/cm^2$. For a high number of melting cycles, the minimum lifetime for the highest energy density only reaches $\tau_{eff} = 6$ μs.

measured minority carrier lifetimes would be expected when removing this portion of the surface layer.
- Most probably a continuous introduction of defects into the treated surface layer occurs, causing the lifetime reduction. If this was the main effect, then a continuous lifetime recovery would be expected, when removing parts of the surface layer.

A further experiment serves to investigate these possibilities. A series of FZ samples $N_A = 5 \times 10^{15}$ cm^{-3} is irradiated on the front side with $D_p = 1.2$ J/cm^2 and $N_{melt} = 2$ and 14. After irradiation, the samples are cleaned and their surfaces are etched slowly in 60% KOH solution at a temperature $T = 20\,^{\circ}$C. At this low temperatures, the etch rate of the solution is low,[17] allowing for a controlled removal of thin surface layers.

Figure 3 depicts the values of τ_{eff} versus the etch depth d_{etch} for the two melt repetitions. With the surface layer being step by step removed, the effective lifetime gradually increases from a minimum of $\tau_{eff} = 280\,\mu$s and $640\,\mu$s ($N_{melt} = 14$ and 2) to $\tau_{eff} \approx 1.2$ ms. The comparison with reference values shows that for $d_{etch} > 300$ nm, the defected layer is completely removed in the case of $N_{melt} = 14$. For $N_{melt} = 2$, only three samples are processed. However, the faster increase of the lifetime τ_{eff} already at low $d_{etch} = 20$ and 80 nm indicates that there exist less and shallower defects for less melt repetitions. This finding is in accordance with the lifetime measurements presented earlier.

SIMS characterization

The above results show that neither defects at the surface nor defects at the melt interface, but defects extending throughout the complete laser treated layer are the major reason for the lifetime reduction. Since we rule out structural defects due to the earlier studies,[12,14] we take a closer look at possibly incorporated impurities, by SIMS. For that purpose, samples are prepared likewise to the lifetime samples above without any dopant layer applied. The pulse energy density

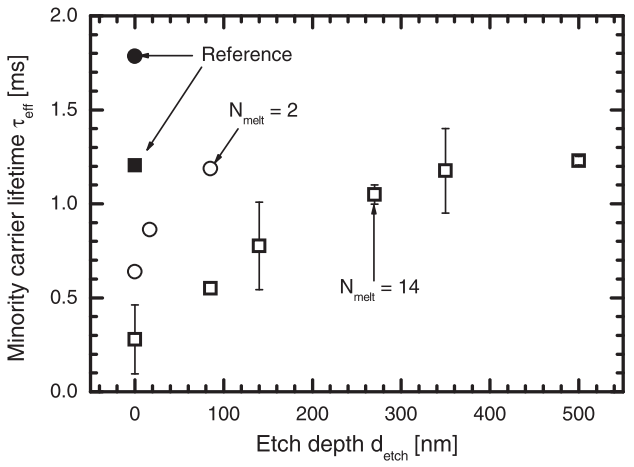

FIG. 3. A stepwise removal of the surface of irradiated samples gradually increases the maximum effective carrier lifetime from $\tau_{eff} = 280\,\mu$s and $640\,\mu$s ($N_{melt} = 14$ and 2) to $\tau_{eff} \approx 1.2$ ms. For the former series, etching approximately 300 nm restores the reference values, indicating that the defected layer has been completely removed. For the latter series, lifetime rises close to reference values already after etching approx. 100 nm.

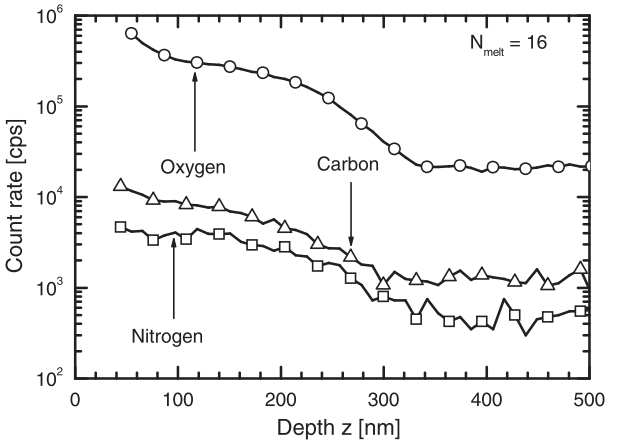

FIG. 4. The laser irradiation incorporates oxygen, carbon, and nitrogen into the silicon up to a depth $z \approx 300$ nm for a pulse energy density $D_p = 1.23$ J/cm^2 and 16 melt repetitions. The measured values for $z < 80$ nm are not reliable due to C, O, N adsorbed at the sample surface.

is $D_p = 1.2$ J/cm^2 and N_{melt} varies. Figure 4 depicts the measured count rates for oxygen (O), carbon (C), and nitrogen (N) as SiN^- ion for 16 fold melting. All three curves have similar shapes, only differing in the absolute count rates. The impurities are taken up to a depth $z \approx 350$ nm. At that depth, the count rate declines to the instruments background level. We attribute the sharp rise of count rates within the first 50 nm to adsorbed C, O, and N at the surface and not to a real incorporation effect.

Figure 5 shows the oxygen count rate converted to absolute concentration values for the sample from Figure 4, together with a different sample irradiated with $N_{melt} = 2$. The maximum concentrations C_{max} amount to $C_{max} \approx 2 \times 10^{19}$ and 3×10^{19} cm^{-3} for $N_{melt} = 2$ and 16, respectively. Furthermore, the profile for 2 melt repetitions is significantly shallower, extending only to $z \approx 200$ nm. Obviously, oxygen is taken up continuously into the silicon with repeated melting, leading to an increase in profile height and depth. The oxygen and nitrogen concentrations detected in this work are in accordance with studies from Hoh[7] and Hameiri.[18]

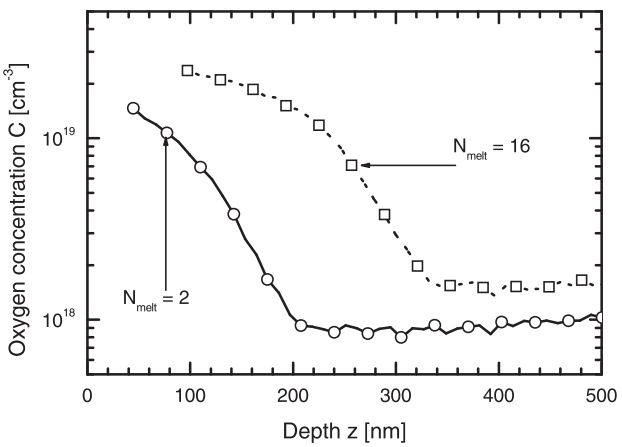

FIG. 5. Converting the arbitrary units of FIG. 4 into absolute concentration values for oxygen yields peak concentrations $C_{max} \approx 3 \times 10^{19}$ cm^{-3} for $N_{melt} = 16$. The second curve shows measured values of a sample irradiated with $N_{melt} = 2$. Here, oxygen is only measured up to $z \approx 200$ nm and with a peak concentration $C_{max} \approx 2 \times 10^{19}$ cm^{-3}.

Optical characterization

Our SIMS measurements reveal O, C, and N to be incorporated into silicon by laser melting. In the past, for non-laser treated samples a multitude of studies investigated the configuration and effects of these three incorporated species. Carbon is known to be part of structural defects in annealed silicon, giving rise to the so called "C-line"[19] and the "G-line"[20] in PL-measurements. Nitrogen is believed to be incorporated, above all, in the kinetics of so called shallow thermal donors (STDs), electrically active defect states that additionally involve oxygen.[21] Oxygen itself is the most widely studied species, being responsible for further donor states, also known as thermal and new thermal donors (TDs and NTDs) [e.g., Refs. 22 and 23], as well as other defect states, such as oxygen precipitates.[24] Some of these structures are optically active and can be detected by FTIR or PL measurements. Therefore, we conduct these measurements on irradiated samples. Once again, the samples are FZ, p-type material with $N_A = 5 \times 10^{15}$ cm^{-3}, to avoid excessive background oxygen contamination as would be present in CZ material. The samples are irradiated with $D_p = 1.3$ J/cm^2 and $2 < N_{melt} < 192$ on both sides. From these parameters, an oxygen diffusion depth of approximately $z \approx 300$ nm on each side can be expected, which represents approximately 0.2% of the whole wafer thickness $w = 300\,\mu$m.

Figure 6 shows the results from an FTIR measurement at liquid helium temperature. A clear peak, which strictly correlates with the number of melting cycles, is seen at a wave number $\lambda^{-1} = 1134$ cm^{-1}. The peak is a typical sign of interstitial oxygen (O_I) in silicon, as examined, e.g., by Hrostowski.[25] This result also corresponds to the findings of Stein and Peercy,[26] who conducted laser annealing experiments with oxygen implanted silicon and found interstitial oxygen, as well as Hahn *et al.*,[22] who likewise detected O_I concentrations in the 10^{19} cm^{-3} range. In our measurements, no other characteristic lines are found in the examined spectrum, above all no evidence for thermal donors, which also exhibit a multitude of infrared active lines. However, as the absorption volume is less than 1% of the whole wafer, a lower concentration of these species could still exist below the detection limit of the instrument.

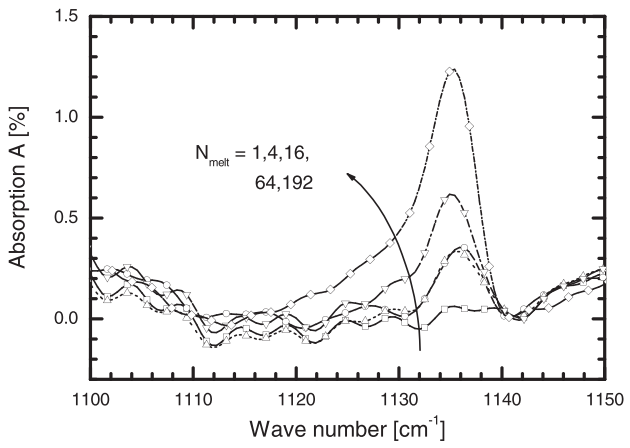

FIG. 6. FTIR characterization shows a clear correlation with the number of melting cycles the sample undergoes and the infrared absorption peak at λ^{-1} 1134 cm^{-1}, which is associated with interstitial oxygen. The magnitude A of the absorption reaches a value $A = 1.3\%$ for the maximally irradiated sample.

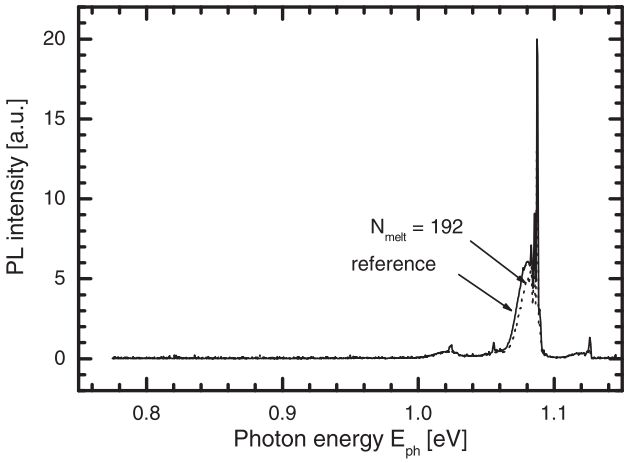

FIG. 7. The comparison of PL-measurements from the untreated reference and one 192-fold irradiated sample shows no observable difference in the resulting spectra. The signal from the irradiated sample is slightly lower around 1.1 eV, which is probably caused by a nm-sized laser induced surface texture. Especially, no evidence for the existence of dislocations (lines D1-D4), oxygen precipitates or other structures can be seen in the signal of the irradiated sample.

Figure 7 shows the results of PL-measurements of the sample with $N_{melt} = 192$ from the above series, compared to a non-irradiated reference sample. The measurements are also taken at liquid helium temperature, with an excitation wavelength $\lambda = 514$ nm. The absorption length L_α for this wavelength is $L_\alpha \approx 1\,\mu$m, so that the detected signal contains much more information from the irradiated layer than the FTIR signal. Except a slightly lower signal, the measured curve of the irradiated sample perfectly matches the reference curve. Above all, neither the well known dislocation lines in the range of 0.8 eV $< E_{PL} <$ 0.99 eV, nor the C, G, and P-lines are present in the measurement. Also certain thermal donors exhibit PL signatures, as described by Tajima[27] or Nakajima.[28] However, these lines cannot be found in the measurement of Figure 7, either. The slight decrease in the intensity probably stems from a minor surface texture that is created by the irradiation.

The result from the PL characterization further backs up our earlier results of the non-existence of one and two dimensional crystal defects inside the irradiated layers, nor any other type of known defects. The FTIR measurements prove that the oxygen found by SIMS is incorporated interstitially. No other lines of thermal donors, carbon or nitrogen related species are detected. Still, some could exist because of the low aerial density of the incorporated species when the whole absorption volume is regarded. To look for any electrically active species, we, therefore, additionally perform ECV measurements on selected samples.

ECV measurements

Figure 8 depicts the results from the measurement of two irradiated p-type FZ samples with $D_p = 1.3$ J/cm^2 and $N_{melt} = 4$ and 16. Clearly, a conductivity change from p-type

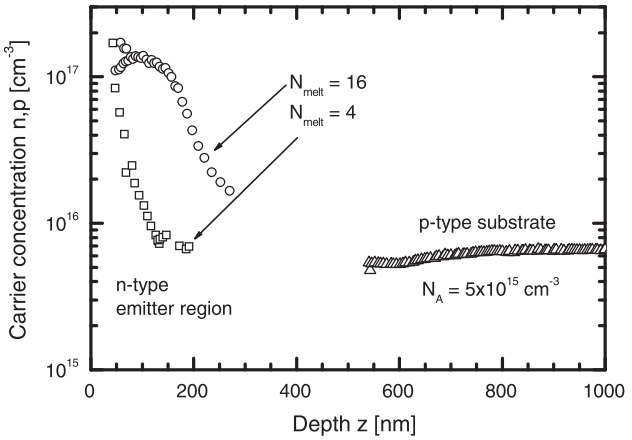

FIG. 8. ECV measurements clearly show an n-type conducting surface layer created on a p-type substrate by irradiation with $N_{melt} = 4$ and 16 at $D_p = 1.3\,J/cm^2$. The behaviour of the profiles with a deeper and more rectangular shape for a higher number of melt repetitions is similar to the measured SIMS oxygen profiles. However, the absolute carrier density measured by ECV is approximately two orders of magnitude lower than the actual oxygen incorporation found by SIMS.

to n-type is observed at the surface, with a maximum concentration $C_{max} \approx 2 \times 10^{17}$ cm^{-3}, extending approximately 200 nm and 300 nm into the substrate for $N_{melt} = 4$ and $N_{melt} = 16$, respectively. The profile for $N_{melt} = 4$ rapidly declines, whereas the sample for $N_{melt} = 16$ approaches a more rectangular shape. The phenomenon of conductivity change upon laser irradiating a p-type substrate was also reported by Mada et al.,[29] who even fabricated pn-junction diodes from the irradiated areas. They, however, ruled out oxygen thermal donors being responsible for the doping, as they did not experience any conductivity change after annealing the samples at 650 °C for 1 h, which they claimed sufficient for the destruction of these donors.

To investigate the thermal stability of the detected conductivity changes, we perform thermal annealing experiments at temperatures $T = 800\,°C$ for 6 h with the ECV measured samples of Figure 8. Interestingly, the n-type doped surface region vanishes and p-type conductivity is re-established throughout the whole sample. Obviously, there is indeed a kind of "thermal donors" created by the irradiation, only their specific type is difficult to analyze. Based on these findings, we prepare three series of lifetime samples from FZ, p-type doped substrates with $N_A = 5 \times 10^{15}$ cm^{-3}. The laser parameters are $D_p = 1.3\,J/cm^2$ and $0 < N_{melt} < 16$. One series is passivated with the same process as described above directly after the irradiation. The other two sets are cleaned thoroughly and then subjected to an annealing step at $T = 600\,°C$ and 800 °C, respectively, before applying the surface passivation. Finally, the effective carrier lifetime τ_{eff} of all three series is measured. Unfortunately, some degradation during the annealing step obscures the results and renders the 800 °C samples useless. The samples annealed at $T = 600\,°C$, however, still show an interesting feature. Figure 9 depicts these results. The reference samples exhibit the well known monotonic lifetime decrease for higher values of N_{melt}, from $\tau_{eff} = 1200\,\mu s$ ($N_{melt} = 0$) to $\tau_{eff} = 40\,\mu s$ ($N_{melt} = 16$). After thermal treatment, there some degradation occurs due to the annealing, as the lifetime of the untreated reference sample drops from $\tau_{eff} = 1300\,\mu s$ to $\tau_{eff} = 400\,\mu s$. The reason is probably some residues not completely removed by the cleaning step. The opposite effect, however, appears for the maximally irradiated sample ($N_{melt} = 16$). Here, a drastic increase of the lifetime from $\tau_{eff} = 40\,\mu s$ to $\tau_{eff} = 250\,\mu s$ is detected. Apparently, the thermal treatment likewise destroys or diminishes the laser induced defects in the sample, which points at a correlation between the n-type doping and the lifetime reduction.

DISCUSSION

The characterization of the laser induced effects turns out to render interesting results. The monotonous reduction of the effective minority carrier lifetime with increasing laser irradiation as well as the likewise monotonous incorporation of oxygen, nitrogen, and carbon, measured by SIMS, are obvious. Quantification of the incorporated oxygen yields high peak concentrations exceeding 10^{19} cm^{-3}. FTIR measurements show that the incorporated oxygen is located on interstitial lattice sites, where no electrical activity is expected. Other lines cannot be identified in the FTIR spectrum, possibly because the total absorption volume is too low for the instrument resolution. A comparison between an irradiated sample with an untreated reference does not show any significant differences in PL measurements. Above all, no lines for dislocations, oxygen precipitates or known thermal donors are present in the signal.

Still ECV measurements clearly show that there indeed exist electrically active species after laser irradiation, causing a conductivity type conversion of the samples from p-type to n-type. The shape of their profiles matches the diffusion profiles of oxygen, only the concentration is approximately two orders of magnitude lower. Thermal annealing at temperatures suitable to destroy the known thermal donors also removes the n-type doping from the samples and additionally leads to a significant recovery of the minority carrier

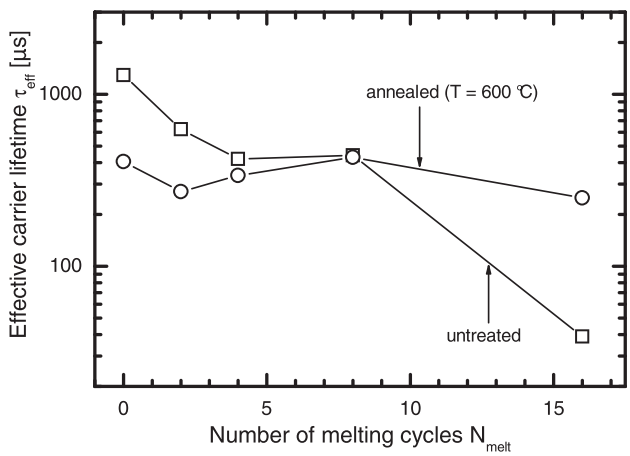

FIG. 9. Annealing the samples irradiated with $D_p = 1.3\,J/cm^2$ and $0 < N_{melt} < 16$ leads to a certain degradation of minority carrier lifetimes, as the reference τ_{eff} drops from $\tau_{eff} \approx 1300\,\mu s$ to $\tau_{eff} \approx 400\,\mu s$ without irradiation. On the contrary, there can be seen a strong influence of the temperature treatment on the lifetime of the sample irradiated with $N_{melt} = 16$. Here, the lifetime drastically increases from $\tau_{eff} = 40\,\mu s$ to $\tau_{eff} = 250\,\mu s$.

lifetime of irradiated samples. Obviously, there indeed exists a type of thermal donors in the irradiated layers, although the standard characterization techniques do not show evidence thereof. Furthermore, most probably, the doping effect and the lifetime reduction have the same origin, as the effect of oxygen donors on the minority carrier lifetime is known from the literature.[30]

Estimation of defect lifetime

Figure 3 shows that the measured effective minority carrier lifetimes are determined solely by the irradiated surface layer, with the laser induced defects being distributed throughout the several 100 nm of irradiated surface layer. Thus, the local lifetimes inside these layers must be fairly low, as the diffusion length $L = \sqrt{D\tau}$ must be in the range of the layer thickness of $z < 1\ \mu$m to cause an effect. Here D denotes the minority carrier diffusion constant.

The laser treatment gives rise to an n-type doping with concentrations $N_D \approx 10^{17}$ cm^{-3}, as evident from Figure 8. The Auger lifetime for $N_D = 10^{17}$ cm^{-3} ranges around $\tau_{Aug} \approx 50\ \mu$s, resulting in a diffusion length $L_{Aug} \approx 300\ \mu$m. This value is in the range of the bulk diffusion length of intermediate quality bulk silicon and would therefore not cause any noticeable recombination inside a several hundred nanometer thin surface layer. Thus, the n-type doping *alone* does not degrade τ_{eff}. In fact, the diffusion length needs to reduce to a few μm to cause an effect on the lifetime. This would be the case for defect lifetimes around or below $\tau_{SRH} \approx 10$ ns, corresponding to a diffusion length $L_{SRH} \approx 3\ \mu$m in n-type doped silicon.

Assessment of junction recombination

The appearance of an n-type layer after laser irradiation leads to the formation of a pn-junction at the surface of the irradiated p-type samples. Extracting the effective surface recombination velocity S_{eff} from the effective minority carrier lifetime as shown in Figure 1 and representing S_{eff} by a saturation current density J_{0e} according to[31]

$$S_{eff} = J_{0e}\frac{N_A + \Delta n}{q n_i^2} \tag{1}$$

gives an estimate for the recombination activity at the induced junction. Thereby, N_A denotes the substrate doping concentration, Δn the excess carrier concentration, q the elementary charge, and n_i the intrinsic carrier concentration. Figure 10 depicts the respective values of the sample sets A-C versus N_{melt}. The relative behaviour of the three curves is similar, with a strong initial rise of J_{0e} up to $N_{melt} = 4$, followed by a roughly constant saturation current density up to $N_{melt} = 16$ and another significant increase for 20 melt cycles. The reason for the distinct increase between $N_{melt} = 16$ and 20 is not clear at this time. The absolute values, however, differ strongly, with 5 fA/cm^2 $< J_{0e} <$ 84 fA/cm^2 for series A, compared to an approximately 10-fold increase fort series C with 105 fA/cm^2 $< J_{0e} <$ 715 fA/cm^2 (for $1 < N_{melt} < 20$). Series B lies in between. As already seen from the lifetime values of Figure 1, a higher substrate doping concentration increases the sensitivity towards the laser treatment, as the absolute saturation current densities roughly reflect the corresponding substrate doping levels. This finding is somehow unexpected, as the properties of the laser irradiated layers should be similar for different wafer types. One possible reason for this different sensitivity could be boron atoms from the substrate doping playing a decisive role in the formation of the laser induced recombination centres. However, the exact mechanism of the defect formation is still under investigation.

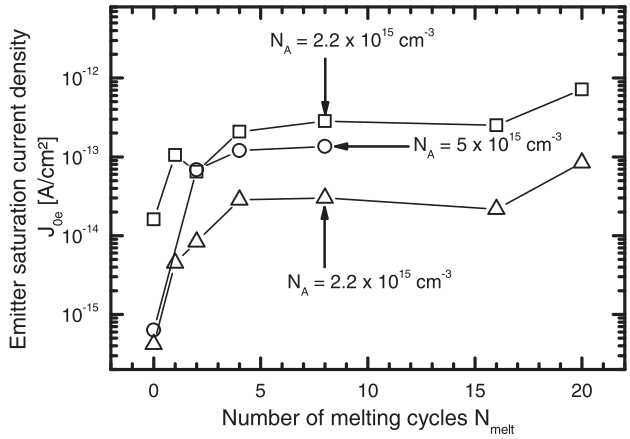

FIG. 10. Representing the effective surface recombination velocities S_{eff} of sample series A-C with saturation current densities J_{0e} shows a similar relative behaviour for the three series. A strong initial rise of J_{0e} up to $N_{melt} = 4$ is followed by a relatively constant saturation current density up to $N_{melt} = 16$ and another increase for $N_{melt} = 20$. The absolute values, however, roughly correspond the respective substrate doping concentrations with 5 fA/cm^2 $< J_{0e} <$ 84 fA/cm^2 for series A and 105 fA/cm^2 $< J_{0e} <$ 715 fA/cm^2 for series C (for $1 < N_{melt} < 20$). Series B lies in between.

Potential impact on laser processed emitters

When the laser process is used together with a "real" emitter, e.g., for creating selectively doped regions in a furnace diffused emitter or creating selectively doped areas in a back junction solar cell, the low SRH lifetime of the introduced defects reduces its performance. The magnitude of this reduction, however, strongly depends on the type and fabrication sequence of the emitter before the laser irradiation, especially on the emitter doping concentration. For a "standard" emitter, the inevitable Auger recombination largely determines its performance. In the case of a laser diffused emitter, there additionally exists laser induced SRH recombination. The resulting minority carrier lifetime

$$\tau_p = \frac{\tau_{Aug} \cdot \tau_{SRH}}{\tau_{Aug} + \tau_{SRH}} \tag{2}$$

is therefore influenced by both Auger and SRH recombination.

Figure 11 illustrates the effect by plotting the Auger lifetime for doping concentrations of $10^{17} < N_D < 10^{21}$ cm^{-3} and the combined Auger and SRH lifetimes for assumed $\tau_{SRH} = 5$, 10, and 20 ns, respectively. Clearly, on the one hand, for emitter doping concentrations $N_D < 10^{19}$ cm^{-3} the effective emitter lifetime is limited by the SRH lifetime. On the other hand, for doping concentrations $N_D > 10^{20}$ cm^{-3}, the influence from the SRH lifetime is virtually irrelevant.

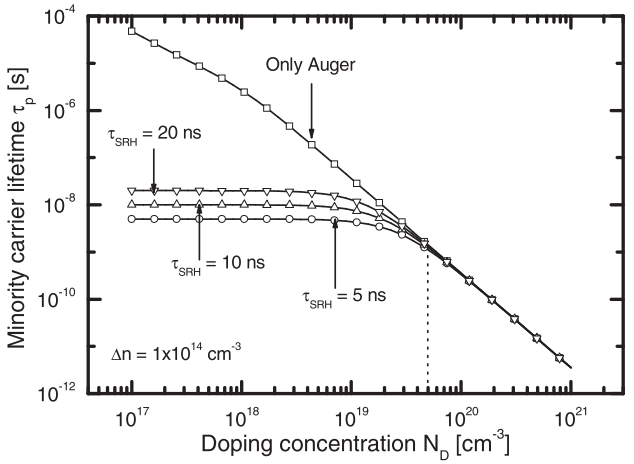

FIG. 11. A laser induced SRH lifetime of $\tau_{SRH} = 5$, 10, or 20 ns influences the resulting minority carrier lifetime τ_p of a diffused emitter up to a doping concentration $C \approx 5 \times 10^{19}$ cm^{-3} (dotted line). For higher doping densities, the Auger lifetime is much lower than the laser induced SRH lifetime, rendering the influence of the laser induced defects virtually irrelevant.

Thus, in high efficiency emitters, which normally feature low peak doping concentrations $C_{max} \approx 10^{19}$ cm^{-3} and rather deep emitter profiles in order to lower surface and Auger recombination, the impact of laser irradiation is likely to be noticeable. This effect was already shown in Ref. 15, where the saturation current densities of emitters with $C_{max} \approx 10^{19}$ cm^{-3} and depths $w \approx 1\,\mu$m increased by a factor of 2 or larger after laser irradiation. Still, even with these defects present, very high open circuit voltages can be achieved, as demonstrated by Eisele et al.[32] On the other hand, industrial solar cell emitters normally feature very high surface doping concentrations $C_{max} > 10^{20}$ cm^{-3}. Here, as Auger lifetimes are much lower, an additional laser doping step would not cause a noticeable effect on the saturation current density. Therefore, a possible negative impact of a local laser irradiation on the performance of industrial type solar cell emitters can be neglected. Furthermore, if the laser doping is used for forming selectively doped regions underneath contacted areas, the emitter saturation current density of these areas will be dominated by the high surface recombination velocity due to the metal contacts. The effect of the laser induced defects will, therefore, be even less relevant. Consequently, the successful implementation of the described laser doping process for the creation of selective emitters for industrial solar cells is under way.[33]

CONCLUSION

Applying the *ipv* laser doping process on bare p-type silicon leads to an incorporation of oxygen, carbon and nitrogen into the melted and recrystallized surface layer. Furthermore, a significant reduction of the effective lifetime of the processed samples is evident, with the magnitude of the lifetime drop corresponding to the applied pulse energy density and the number of melt repetitions. The induced defects are distributed throughout the laser treated layer, with their incorporation depth corresponding to the incorporation depth of the abovementioned impurities. Whereas earlier findings of the absence of structural defects are corroborated, ECV characterization shows that the irradiation gives rise to a conductivity type conversion at the surface. As this phenomenon was already discovered before, there is a strong indication that the impurity incorporation is the reason for both lifetime reduction and n-type doping. Most probably, the incorporated oxygen is mainly responsible for the two effects, as oxygen is known to act as n-type dopant under certain circumstances, as well as to strongly influence minority carrier lifetime, even if the specific type of defect could not be identified in this study.

A rough estimation determines the local SRH lifetime inside the surface layer to $\tau_{SRH} \approx 10$ ns. This comparably low lifetime is prone to deteriorate the performance of irradiated high efficiency emitters, but can be virtually neglected when dealing with irradiated industrial emitters as well as underneath metal contacts. Thus, there is no indication against the use of the *ipv* laser process in an industrial environment, e.g., for the formation of selective solar cell emitters.

ACKNOWLEDGMENTS

We gratefully acknowledge the PL and FTIR measurements as well as the help with their interpretation from Prof. J. Weber and M. Allardt, University of Dresden. A big "thank you" also goes to Dr. R. Kopecek, ISC, Konstanz for ECV measurements.

[1]E. Fogarassy, R. Stuck, J. J. Grob, and P. Siffert, J. Appl. Phys. **52**, 1076 (1981).
[2]T. Sameshima, S. Usuzi, and M. Sekiya, J. Appl. Phys. **62**, 711 (1987).
[3]T. F. Deutsch, J. C. C. Fan, G. W. Turner, R. L. Chapman, D. J. Ehrlich, and R. M. Osgood, Appl. Phys. Lett. **38**, 144 (1981).
[4]C. W. White, S. R. Wilson, B. R. Appleton, and F. W. Young Jr., J. Appl. Phys. **51**, 738 (1980).
[5]J. C. Wang, R. F. Wood, and P. P. Pronko, Appl. Phys. Lett. **33**, 455 (1978).
[6]D. L. Parker, F.-Y. Lin, S.-J. Zhu, D. K. Zhang, and A. W. Porter, IEEE Trans. Electron Devices **30**, 1322 (1983).
[7]K. Hoh, H. Koyama, K. Uda, and Y. Miura, Jpn J. Appl. Phys. **19**, L375 (1980).
[8]M. Berti, L. F. Donná dalle Rose, A. V. Drigo, C. Cohen, J. Sijeka, C. G. Bentini, and E. Jannitti, Phys. Rev. B **34**, 2346 (1986).
[9]M. A. Green, *High Efficiency Silicon Solar Cells* (Trans Tech Publications, Aedermannsdorf, 1987).
[10]P. J. Verlinden, R. A. Sinton, K. Wickham, R. A. Crane, and R. M. Swanson, in *Proceedings of the 14th European Photovoltaic Solar Energy Conference*, edited by H. Ossenbrink, P. Helm, and H. Ehmann (Stephens & Associates, Bedford, United Kingdom, 1997), p. 96.
[11]T. Frieß, A. Teppe, J. Olkowska-Oetzel, W. Zimmermann, C. Voyer, A. Esturo-Bretón, J. Isenberg, S. Keller, D. Hammer, M. Schmidt, and P. Fath, in *Proceedings of the 25th European Photovoltaic Solar Energy Conference*, edited by G. F. De Santi, H. Ossenbrink, and P. Helm (WIP-Renewable Energies, München, Germany, 2010), p. 2164.
[12]J. R. Köhler, M. Ametowobla, and A. Esturo-Bretón, in *Proceedings of the 20th European Photovoltaic Solar Energy Conference*, edited by W. Palz, H. Ossenbrink, P. Helm (WIP-Renewable Energies, München, Germany, 2005), p. 1162.
[13]K. Ohmer, Y. Weng, J. R. Köhler, H. P. Strunk, and J. H. Werner, IEEE J. Photovoltaics **1**, 183 (2011).
[14]M. Ametowobla, J. R. Köhler, A. Esturo-Bretón, and J. H. Werner, in *Proceedings of the 21st European Photovoltaic Solar Energy Conference*, edited by J. Poortmanns, H. Ossenbrink, E. Dunlop, and P. Helm (WIP, Munich, 2006), p. 1440.
[15]M. Ametowobla, J. R. Köhler, A. Esturo-Bretón, and J. H. Werner, in *Proceedings of the 22nd European Photovoltaic Solar Energy Conference*, edited by W. Palz, H. Ossenbrink, and P. Helm (American Institute of Physics, München, Germany, 2007), p. 1403.

[16]W. Kern and D. A. Puotinen, RCA Rev. **31**, 187 (1970).
[17]H. Seidel, J. Electrochem. Soc. **137**, 3612 (1990).
[18]Z. Hameiri, T. Puzzer, L. Mai, A. B. Sproul, and S. R. Wenham, Prog. Photovoltaics **19**, 391 (2011).
[19]K. Thonke, G. D. Watkins, and R. Sauer, Solid State Commun. **51**, 127 (1984).
[20]J. Weber, R. J. Davis, and H.-U. Habermeier, Appl. Phys. A **41**, 175 (1986).
[21]M. Suezawa, K. Sumino, H. Harada, and T. Abe, Jpn. J. Appl. Phys. **25**, L859 (1986).
[22]S. Hahn, H. J. Stein, S. C. Chatas, and F. A. Ponce, J. Appl. Phys. **72**, 1758 (1992).
[23]W. Götz, G. Pensl, and W. Zulehner, Phys. Rev. B **46**, 4312 (1992).
[24]A. Borghesi, B. Pivac, A. Sassella, and A. Stella, J. Appl. Phys. **77**, 4169 (1995).
[25]H. J. Hrostowski and R. H. Kaiser, Phys. Rev. **107**, 966 (1957).
[26]H. J. Stein and P. S. Peercy, Mater. Res. Soc. Symp. Proc. **13**, 229 (1983).
[27]M. Tajima, A. Kanamori, and T. Iizuka, Jpn. J. Appl. Phys. **18**, 1401 (1979).
[28]H. Nakayama, T. Nishino, and Y. Hamakawa, Appl. Phys. Lett. **38**, 623 (1981).
[29]Y. Mada and N. Inoue, Appl. Phys. Lett. **48**, 1205 (1986).
[30]D. Karg, G. Pensl, and M. Schulz, Phys. us Solidi **222**, 379 (2000).
[31]S. C. Jain and R. Muralidhan, Solid-State Electron **24**, 1147 (1981).
[32]S. Eisele, T. Röder, J. R. Köhler, and J. H. Werner, Appl. Phys. Lett. **95**, 133501 (2009).
[33]J. R. Köhler, P. Grabitz, S. Eisele, T. Röder, and J. H. Werner, in *Proceedings of the 24th European Photovoltaic Solar Energy Conference*, edited by W. C. Sinke, H. Ossenbrink, and P. Helm (WIP-Renewable Energies, München, Germany, 2009), p. 1847.